Available online at www.sciencedirect.com
ScienceDirect
Superlattices and Microstructures 40 (2006) 125–136
Superlattices and Microstructures
www.elsevier.com/locate/superlattices

Strain and piezoelectric fields in embedded quantum wire arrays

F. Han[a], E. Pan[a], J.D. Albrecht[b,*]

[a] *University of Akron, Akron, OH 44325, United States*
[b] *Air Force Research Laboratory, Wright-Patterson Air Force Base, OH 45433, United States*

Received 6 April 2006; received in revised form 26 May 2006; accepted 12 June 2006
Available online 27 July 2006

Abstract

Utilizing a recently developed exact closed-form solution for a single polygonal quantum wire (QWR) inclusion problem, we theoretically investigate the elastic strain and electric fields induced by QWR arrays embedded in GaAs. We consider arrays ranging from 1×1 to 7×7 QWRs embedded in infinite substrates and up to 4×7 QWRs in half space substrates where the wires are near a surface. Our results for the infinite substrate indicate that although the elastic fields within any single QWR are similar to the fields in the other wires with only a weak dependence on the number of QWRs, the electric fields (both inside and outside the QWRs) can be significantly different for different array sizes. Due to the existence of the free surface, the half space solutions show that the elastic and electric fields both inside of and outside of the QWRs depend significantly on the number of QWRs, again with the electric field having the stronger dependence. A detailed analysis of the strain and electric fields for embedded QWR arrays is presented and the results could impact the design of proposed strain-modulated electronic devices.

Keywords: Piezoelectric nanostructures; Polygonal inclusion; Strained quantum wire

1. Introduction

Embedded quantum wires (QWRs) are semiconductor structures with electron confinement in two dimensions most often achieved by using materials of different band gaps. The structures are either directly grown through self-assembly or fabricated such that long (∼1 μm) and

* Corresponding address: Air Force Research Laboratory, SNDD, Building 620, 2241 Avionics Circle, Wright Patterson AFB, OH 45433, United States. Tel.: +1 937 255 1874x3509; fax: +1 937 255 8656.
E-mail addresses: pan2@uakron.edu (E. Pan), john.albrecht@wpafb.af.mil (J.D. Albrecht).

0749-6036/$ - see front matter © 2006 Elsevier Ltd. All rights reserved.
doi:10.1016/j.spmi.2006.06.002

narrow (∼10s of nm) sections of semiconductor are surrounded by a cladding of a larger band gap material. The embedded wire situation results in key differences in physical behavior and is in contrast to free-standing or etched QWRs which are nanostructures surrounded at least partially by vacuum in order to achieve strong confinement. Whereas the etched QWRs are not mechanically stressed on all sides, the embedded wires usually exhibit large strain fields owing to the inevitable structural mismatch between the crystalline wire material and its surroundings. Another key difference is that the embedded wires can be electronically coupled at larger interwire spacings because the typical charge carrier confinement is far weaker than that provided by the semiconductor–vacuum interface present for etched wires.

Embedded wire arrays can be separated into the two main categories of infinite space and half space substrates, each with distinct experimental realizations and theoretical treatments [1–3]. The infinite substrate case corresponds to the physical situation where a self-organization process results in embedded vertical wires orthogonal to the growth surface. Recently, vertical embedded arrays have been proposed for a device structure to provide an efficient carrier extraction mechanism in QWR solar cells [4]. The half space substrate or 'buried wire' case corresponds to the situation where horizontal wires are defined, for example, lithographically from epitaxial films and subsequently overgrown to result in embedded wires oriented in the plane of the epitaxial growth surface.

The inevitable strain and electric fields in nanoscale semiconductor structures induced by the structural boundaries of QWRs have been extensively investigated because the presence of and magnitude of these fields are crucial for understanding the electronic and optical performance [5]. Analytical studies of the strain fields of embedded QWRs are mostly restricted to single wires where the substrate is further treated as a purely elastic solid [6–8]. In other work, some recent advances on treating analytically size-dependent strain [9] and on nonuniform misfit eigenstrain [10] have been reported. Nanostructures can be self-organized layer-by-layer and also can be grown with different crystallographic orientations using materials (such as the group III-nitrides [11]) with a broad range of polarization, mechanical, and electronic properties. Therefore, there is growing interest in computational descriptions of strong electromechanical coupling [12–14], local strain fields [15–18] and the impact of strain on confined electronic states [19].

In this paper, we give an analytical continuum treatment of arrays of closely-spaced QWRs including polarization effects arising from the piezoelectric material response to elastic strain fields. The core of our formalism is a recently reported closed-form solution for a single QWR within a piezoelectric substrate [20] that is extended to the array case for treating multiple QWRs. Though the QWR geometry and materials can in general be arbitrary, the straightforward square shaped QWR in GaAs is assumed in the present analysis of the induced elastic and electric fields and of the interaction due to multiple QWRs. Both infinite and half space substrates with growth orientations of (001) and (111) are considered. The size of each QWR is 4 nm × 4 nm, and the wires are arrayed in 1×1, 3×3, 5×5, and 7×7 patterns for the full-space and 1×1, 2×3, 3×5, and 4×7 patterns for the half space substrate cases. In what follows, we will first describe the problem in more detail with a brief development of the necessary equations for the induced strain and electric fields. Then numerical examples are presented in terms of fields along specific cut lines and contour plots over the space of the structure. Finally, conclusions are drawn on the QWR array induced elastic and piezoelectric features.

2. Problem description

In order to provide concrete examples of our general theory, we assume for the present discussion that simple arrays of infinitely long QWRs with square cross-section are embedded

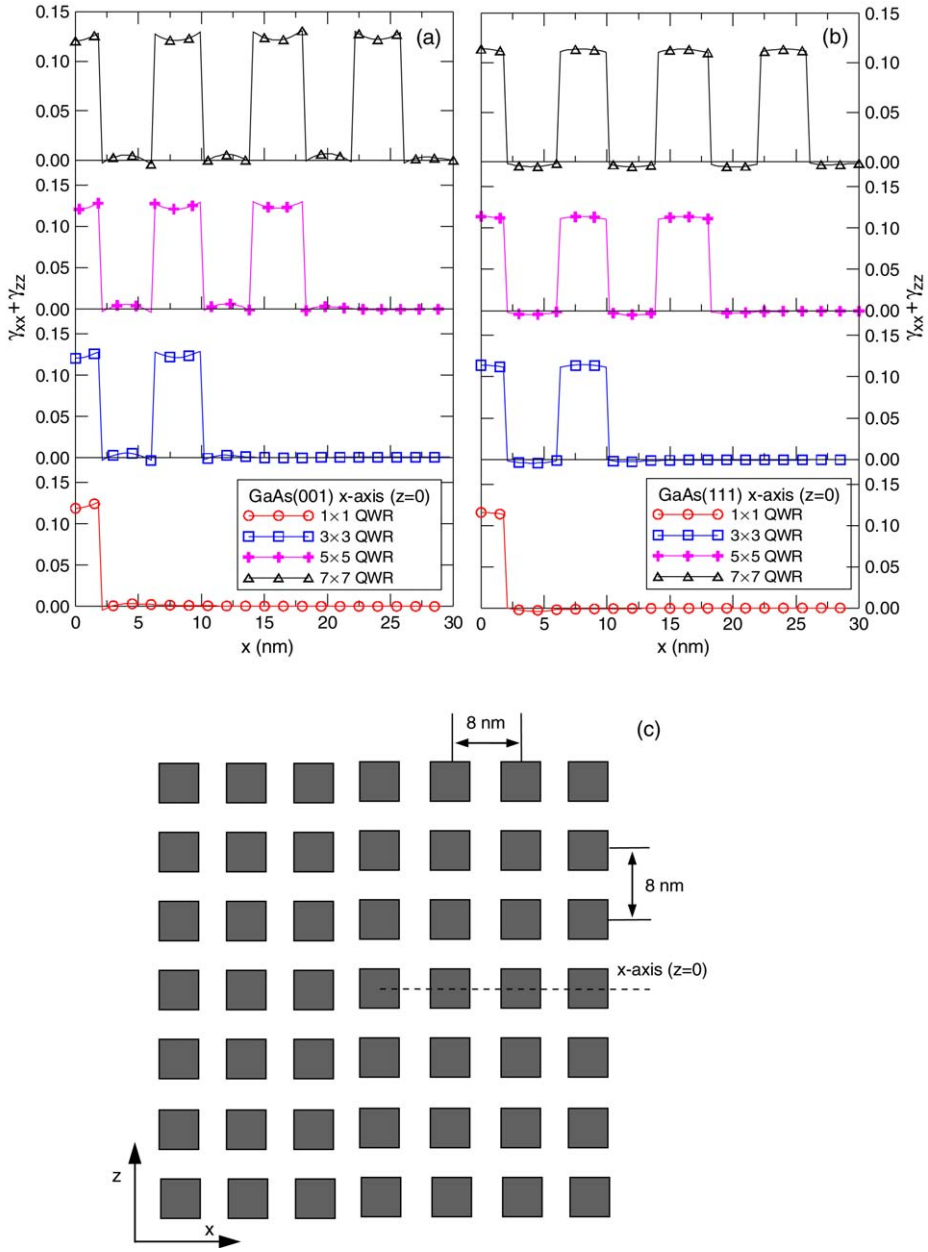

Fig. 1. Variation of the hydrostatic strain for QWR arrays buried in (a) (001)-oriented and (b) (111)-oriented GaAs substrates. Panel (c) gives the geometric layout of the QWR arrays in an infinite space and the dashed line indicates the location of the cut line $z = 0$ for the field calculations of Figs. 1 and 3.

in either (001)-oriented or (111)-oriented GaAs substrates. Each QWR has dimensions of 4 nm × 4 nm and the center-to-center wire distance is 8 nm as shown in Fig. 1(c). The half space substrate case is distinguished from the infinite one by the presence of a free surface 2 nm from the top row of the array as shown in Fig. 4(d). The lattice misfit strain within the wire is

hydrostatic, i.e., $\gamma^*_{xx} = \gamma^*_{yy} = \gamma^*_{zz} = (a - a_o)/a_o$ where a and a_o are the lattice constants in the QWR and surrounding material, respectively. In our numerical examples $\gamma^*_{xx} = 0.07$ which corresponds to the common nanostructure combination of InAs embedded in GaAs. The imposed eigenstrain due to lattice mismatch gives an upper bound on the strain present in the QWR. The strain fields would in reality be decreased by the presence of any plastic deformations such as dislocations or other lattice defects often present in overgrown cladding layers, especially for lattice mismatches greater than 1%.

The elastic properties for modeling GaAs (001) are $C_{11} = 118$, $C_{12} = 54$, and $C_{44} = 59$ GPa. The piezoelectric constant and permeability for GaAs (001) are, respectively, $e_{14} = -0.16$ C/m^2 and $\varepsilon_{11} = 12.42\varepsilon_o$. For (001)-oriented structures, the global coordinates x, y, and z are coincident with the crystalline axes and for (111)-oriented structures the x-axis is along $[11\bar{2}]$, the y-axis along $[\bar{1}10]$, and the z-axis along [111] directions of the GaAs crystal structure (this coordinate system was adopted for single nanostructures in Ref. [18]). The boundary condition on the surface for the half space case is assumed to be traction-free and insulating [21]. The specific QWR arrays are 1×1, 3×3, 5×5, and 7×7 wires for infinite substrates and 1×1, 2×3, 3×5, and 4×7 wires for half space substrates. The dashed lines in Fig. 1(c) and Fig. 4(d) indicate the specific locations for which the induced fields will subsequently be plotted and analyzed in detail.

For a QWR of polygonal shape within either an infinite or half space substrate, the lattice misfit induced strain and electric fields can be expressed analytically in closed form. While we briefly list these induced fields below, the complete derivation can be found in Ref. [20]. For an arbitrary side (line segment) of the polygon extending from the point (x_1, z_1) to (x_2, z_2), the outward normal components $n_i(x)$ are constants, given by

$$n_1 = (z_2 - z_1)/\ell, \qquad n_2 = -(x_2 - x_1)/\ell \tag{1}$$

where $\ell = \sqrt{(x_2 - x_1)^2 + (z_2 - z_1)^2}$ (or the side length of the polygon). The strain and electric fields due to this side of the QWR polygon were found to be [20] (α, $\beta = 1$ and 3 corresponding to the x- and z-components).

$$\begin{aligned}\gamma_{\beta\alpha}(\mathbf{r}) \;=\; & \frac{1}{2} n_i C_{iJLm} \gamma^*_{Lm} \frac{\ell}{\pi} \mathrm{Im} \left\{ A_{JR} h_{R,\alpha}(\mathbf{r}) A_{\beta R} + \sum_{\nu=1}^{4} A_{JR} g^{\nu}_{R,\alpha}(\mathbf{r}) Q^{\nu}_{R\beta} \right\} \\ & + \frac{1}{2} n_i C_{iJLm} \gamma^*_{Lm} \frac{\ell}{\pi} \mathrm{Im} \left\{ A_{JR} h_{R,\beta}(\mathbf{r}) A_{\alpha R} + \sum_{\nu=1}^{4} A_{JR} g^{\nu}_{R,\beta}(\mathbf{r}) Q^{\nu}_{R\alpha} \right\}\end{aligned} \tag{2}$$

$$\gamma_{2\alpha}(\mathbf{r}) = \frac{1}{2} n_i C_{iJLm} \gamma^*_{Lm} \frac{\ell}{\pi} \mathrm{Im} \left\{ A_{JR} h_{R,\alpha}(\mathbf{r}) A_{2R} + \sum_{\nu=1}^{4} A_{JR} g^{\nu}_{R,\alpha}(\mathbf{r}) Q^{\nu}_{R2} \right\} \tag{3}$$

$$E_{\alpha}(\mathbf{r}) = -n_i C_{iJLm} \gamma^*_{Lm} \frac{\ell}{\pi} \mathrm{Im} \left\{ A_{JR} h_{R,\alpha}(\mathbf{r}) A_{4R} + \sum_{\nu=1}^{4} A_{JR} g^{\nu}_{R,\alpha}(\mathbf{r}) Q^{\nu}_{R4} \right\} \tag{4}$$

where summation over repeated indices is implied and where the index values range from 1 to 3 for the lowercase indices i, m and from 1 to 4 for the upper case indices J, L. The Im stands for the imaginary part of the complex function. While C_{iJLm} are the extended material coefficients (elastic, piezoelectric, and permeability), the matrices A and Q in Eqs. (2)–(4) are functions of these coefficients. Finally matrices h and g are functions of the arbitrary field point $\mathbf{r} = (x, z)$, and are given in Ref. [20]. We point out that these expressions of the strain and electric fields are

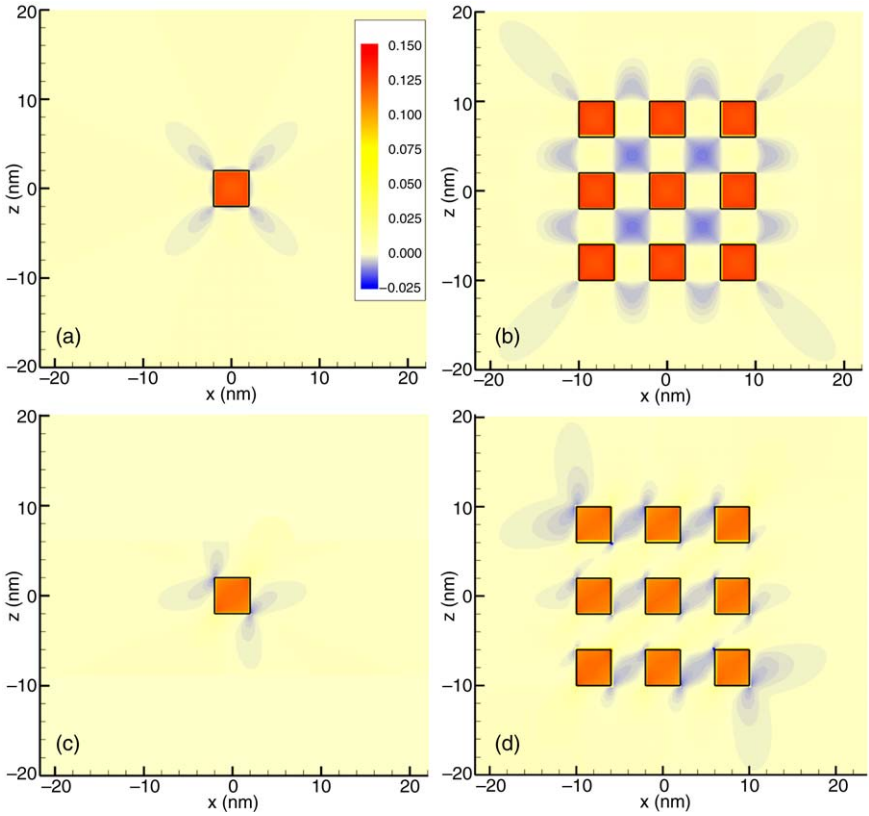

Fig. 2. Contour plots of total hydrostatic strain for QWR arrays buried in infinite spaces. (a) 1 × 1 and (b) 3 × 3 arrays in (001)-oriented; (c) 1 × 1 and (d) 3 × 3 arrays in (111)-oriented GaAs substrates.

for the half space substrate case with the first terms (proportional to the matrix h) being simply the results for the corresponding infinite substrate case.

The particular fields in Eqs. (2)–(4) are the induced strain and electric fields by one side of the QWR polygon. In order to find the induced fields due to the contributions of the whole QWR polygon, we simply add the results from all sides of the polygon together. Similarly, for the multiple QWR case (or QWR array), we add the contributions from all the QWR polygons. For simplicity, in this paper the simple inclusion model is followed, which means that the elastic properties of the buried nanostructure are taken to be those of the surrounding matrix. In other work, the error introduced by this assumption versus including the local differences in the elastic properties of the wire for a GaAs-based system was found to be about 10% inside of or close to the QWR region [22]. These approximations are likely to be smaller effects than the underlying assumption that no dislocations or other strain-relieving extended defects are present.

3. Calculated results and analysis

3.1. QWR array in infinite substrate space

Fig. 1(a) and (b) show the variation of the hydrostatic strain along the positive x-axis for QWR arrays 1 × 1 to 7 × 7 in infinite space GaAs (001) and (111) substrates, respectively.

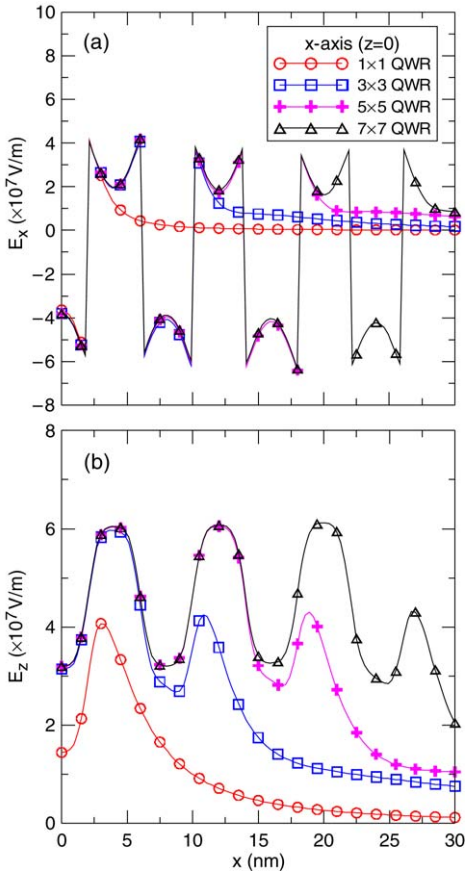

Fig. 3. Variation of electric field components E_x (a) and E_z (b) along the x-axis [$z = 0$ as shown in Fig. 1(c)] for the case of QWR arrays buried in infinite space (111)-oriented substrates.

The corresponding geometry and coordinates are sketched in Fig. 1(c). It is clearly shown in Fig. 1 that the hydrostatic strain inside the QWR is nearly the same for different QWR array cases whilst those outside the QWR are slightly different. We further remark that the induced hydrostatic strain inside the QWR is large, dominated by the misfit strain and therefore relatively insensitive to the number of wires in the particular array. On the other hand, the calculated strain fields in the cladding outside of the QWR regions are more strongly influenced by the number of wires in the array. It is also observed that the distribution of the hydrostatic strain inside the QWR is different for the two substrate cases. While the strain curve inside the QWR is curved down for the (001) case, it is curved up for the (111) substrate case. The magnitude inside the QWR of (001) is slightly larger than that inside the QWR of (111). The induced hydrostatic strain inside the QWR is smaller than the preexisting misfit strain (0.14 for the misfit hydrostatic strain) due to the strain relaxation to the substrate.

The hydrostatic strain contours induced by QWR arrays within an infinite cladding are plotted in Fig. 2. Panels (a) and (b) compare the single (1×1) QWR result to the 3×3 array for the (001) substrate and panels (c) and (d) are for the corresponding results in the (111)-oriented substrate. We observe again that the hydrostatic strain distributions for the two orientations are different,

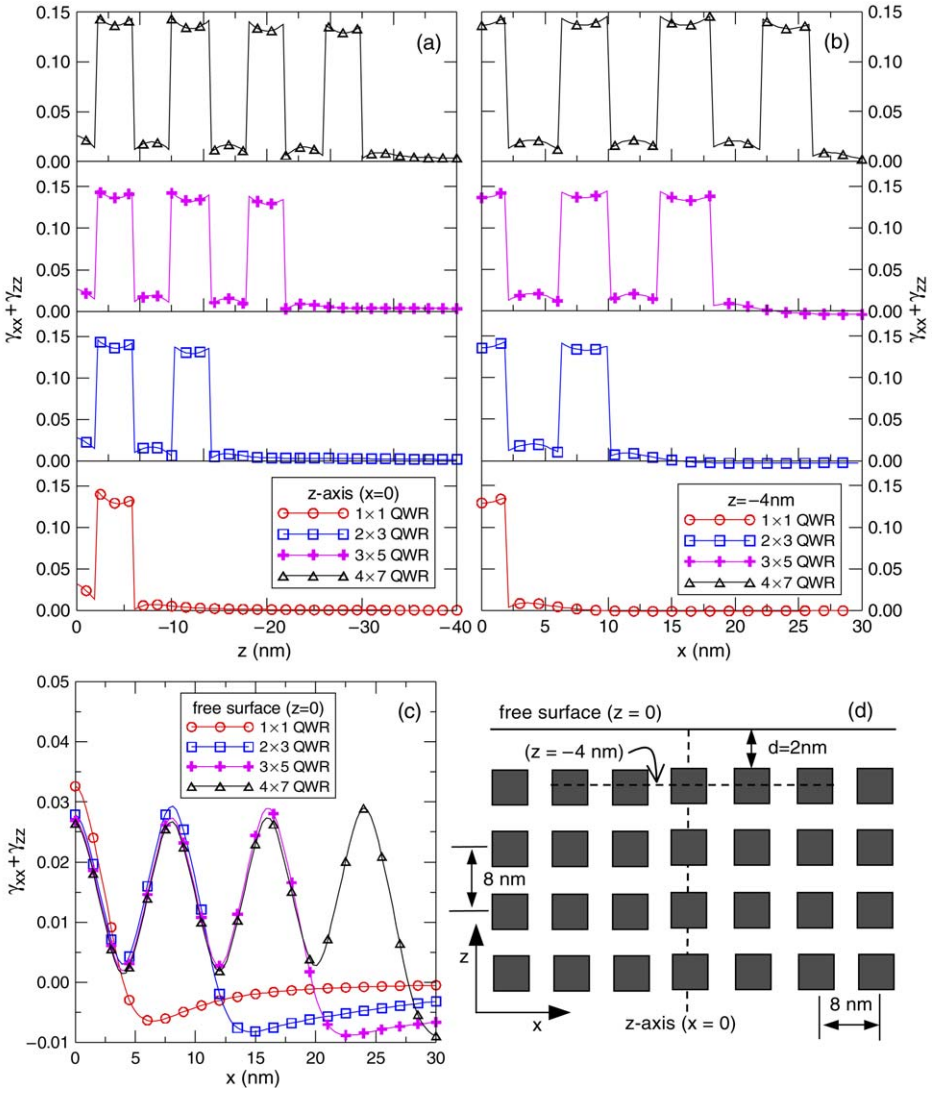

Fig. 4. Variation of the hydrostatic strain for QWR arrays buried in half space (001)-oriented substrates. Hydrostatic strain is plotted for cut lines (a) along the z-axis $x = 0$, (b) along the horizontal line $z = -4$ nm, and (c) along the free surface $z = 0$. Panel (d) gives the geometric layout of the QWR arrays in a half space and the dashed lines indicate the locations for the field calculations of Figs. 4–8.

with even a logarithmic singularity existing at the corners of the GaAs (111) QWR. More details with regard to the corner singularities in the strain fields can be found in Ref. [20].

In a recent calculation, it was predicted that QWRs embedded in (111)-oriented GaAs could experience large polarization electric fields induced by strain effects [18]. However, we have found no previous reports of the induced electric fields in QWR arrays where the wires are close enough to experience common strain fields. Fig. 3 presents the electric field (E_x and E_z) distribution along the positive x-axis (Fig. 1(c)) in infinite substrate GaAs (111) due to QWR arrays 1×1 to 7×7. It is extremely interesting that while the E_x-component within the QWR is

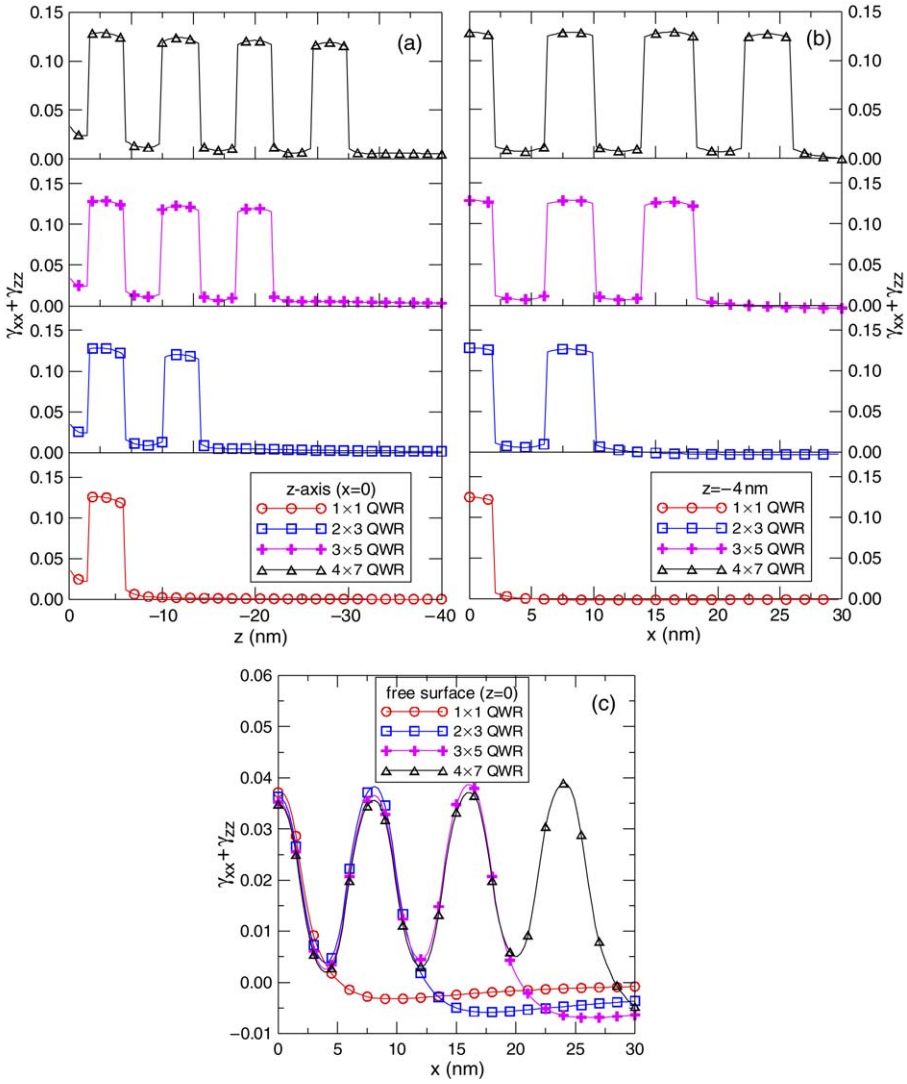

Fig. 5. Variation of the hydrostatic strain for QWR arrays buried in half space (111)-oriented substrates. Hydrostatic strain is plotted for cut lines (a) along the z-axis $x = 0$, (b) along the horizontal line $z = -4$ nm, and (c) along the free surface $z = 0$. The cut lines are shown schematically in Fig. 4(d).

relatively independent of the number of QWRs (Fig. 3(a)), just like the strain distribution within the QWR, the E_z-component depends strongly on the pattern of QWRs (Fig. 3(b)).

3.2. QWR array in half space substrate

Having studied the elastic and electric fields in infinite substrates GaAs (001) and GaAs (111), we now look at the case where the QWR arrays are within a half space substrate and are close to a free surface. For this case, the surface boundary condition is assumed to be traction-free and electrically insulating [21]. In our illustrative numerical examples the distance of the first row of

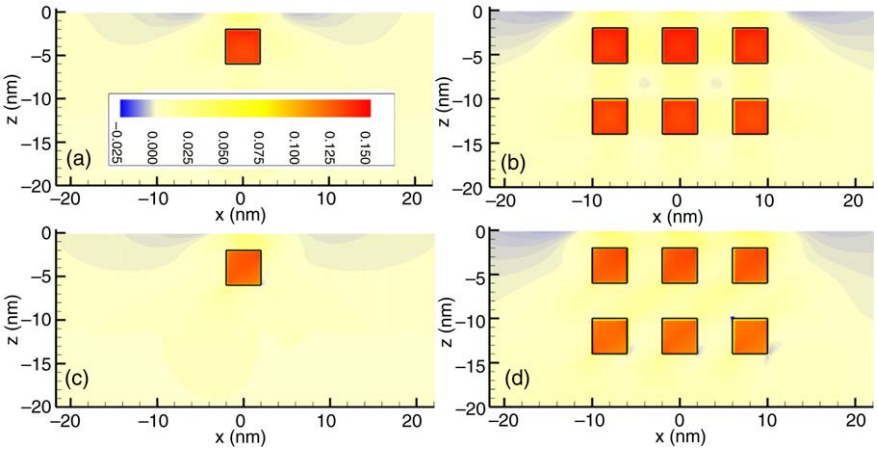

Fig. 6. Contour plots of total hydrostatic strain for QWR arrays buried in half spaces. (a) 1 × 1 and (b) 3 × 3 arrays in (001)-oriented; (c) 1 × 1 and (d) 3 × 3 arrays in (111)-oriented GaAs substrates.

the QWR array to the surface is at $d = 2$ nm as shown in Fig. 4(d). The QWR spacing is the same as for the infinite substrate case so that the QWRs are separated by 8 nm (Fig. 4(d)) from center to center.

Fig. 4 displays the hydrostatic strain variations along three different lines in the half space GaAs (001) substrate. While Fig. 4(a) shows the variation of the hydrostatic strain along the z-axis (for $x = 0$), Fig. 4(b) and (c) are those along the horizontal line at $z = -4$ nm (which is along the center of the first row of the QWR array) and along the free surface ($z = 0$), respectively. It is apparent that the elastic fields both inside and outside the QWR have been increased by the free surface condition, combined with the interaction among QWRs. This feature is particularly clear for the elastic strain close to the free surface where, for instance, the hydrostatic strains inside the QWR can be larger than the hydrostatic misfit strain ($\gamma^*_{xx} + \gamma^*_{zz} = 0.14$) as shown in Figs. 4(a)–(b). Furthermore, due to the existence of the free surface, the strain fields inside and outside the QWR are now clearly different for different numbers of QWRs as seen in Figs. 4(a)–(c). The corresponding hydrostatic strain distributions within the (111)-oriented substrates are shown in Fig. 5. Again, similar features can be observed except that the strain distribution is not symmetric about $x = 0$ as it is for the (001) case.

Fig. 6 shows the contour of the hydrostatic strain in the half space substrate GaAs, with QWR array 1 × 1 in (a) and 3 × 3 in (b) of GaAs (001), and QWR array 1 × 1 in (c) and 3 × 3 in (d) of GaAs (111). Comparing these contours to those in the corresponding infinite substrate (in Fig. 2), we observed that the free surface increases the magnitude and alters the distribution of the strain fields. The effect of the substrate orientation on the strain distribution is also apparent by comparing Fig. 6(a) and (b) to (c) and (d), respectively, the biggest difference being the symmetry displayed in Fig. 6(a) and (b) versus the asymmetry of the fields in Fig. 6(c) and (d).

Fig. 7 shows the distributions of the electric field components E_x and E_z along the free surface of the half space substrate GaAs (111) for QWR arrays 1×1 to 4×7. The electric field distribution is strongly dependent on the pattern and number of QWRs, with the main difference identified for the field outside the QWRs (e.g., Fig. 7(b)). Finally, Fig. 8 shows the variation of the electric field (E_x and E_z) along the z-axis in the half space (111)-oriented substrates. Fig. 8(a) and (b) clearly show the correlation between the number of QWRs and the electric field distribution, and this

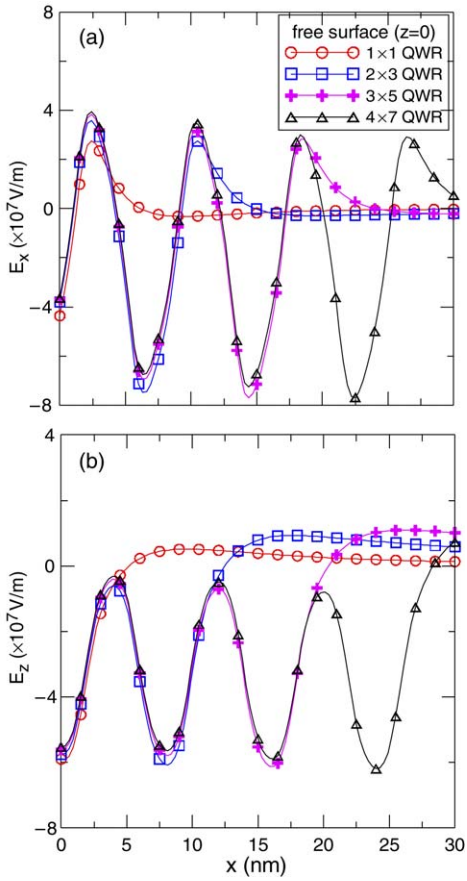

Fig. 7. Variation of electric field components E_x (a) and E_z (b) along the free surface [$z = 0$ as shown in Fig. 4(d)] for the case of QWR arrays buried in half space (111)-oriented substrates.

result could be useful for the design of QWR-containing regions in electronic or optoelectronic devices.

4. Discussion

A recent exact closed-form solution for a single QWR is extended to the QWR array case where each QWR has a square cross-section. The QWR array can be within an infinite substrate or a half space substrate. The induced elastic and electric fields are calculated for the substrate comprised of (001)-oriented and (111)-oriented GaAs. Starting from single wires, a series of QWR arrays up to 7×7 patterns for the infinite space substrate and 4×7 patterns for the half space substrate were studied theoretically. Comparing the induced field within the infinite substrate to that in the half space substrate, we observed that the existence of the free surface can greatly increase the magnitude of the induced elastic and electric fields. It is particularly interesting that even for very close interwire spacings, the number of QWRs in the pattern has only a slight influence on the elastic fields present inside the QWRs. While different numbers of QWRs do strongly affect the elastic field outside the wires, these fields are of course much

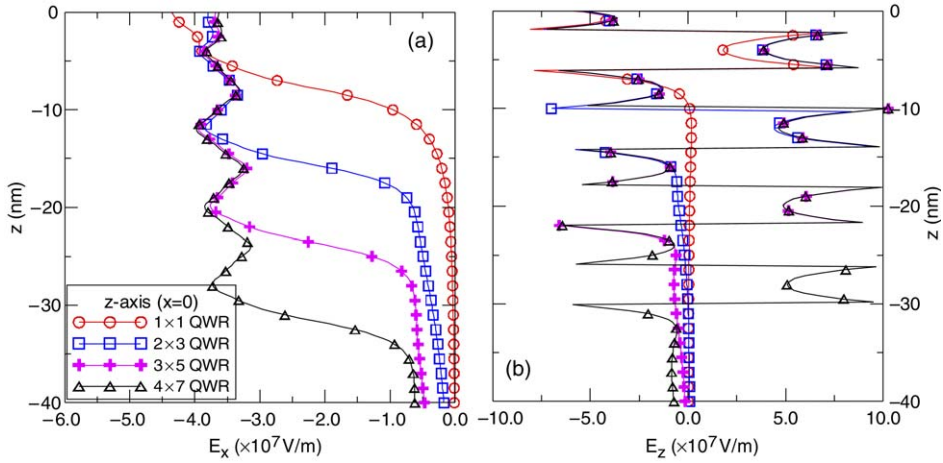

Fig. 8. Variation of electric field components E_x (a) and E_z (b) along the z-axis [$x = 0$ as shown in Fig. 4(d)] for the case of QWR arrays buried in half space (111)-oriented substrates.

smaller in magnitude than those inside the wires. In contrast, and perhaps most important for electronic device applications, the electric fields depend strongly on the number of QWRs in the pattern and variations in the electric field distributions can clearly be observed both inside of and outside of the QWRs as opposed to the relative insensitivity of the strain field features inside the QWR to the details of the array.

The central reason that the electric field distribution is more sensitive to the QWR array configuration is that the large lattice misfit strain present inside the wires dominates the total strain profile whereas the electric field distribution arises from variations in the induced polarization and the surface boundary conditions. The net effect is that for all of the strain distributions in every array we considered, the misfit strain inside the wires is changed in only a minor way by the elastic response of the system. This feature is evident by the uniformity of the strain contour plots which clearly show that inside the wires the total hydrostatic strain is very close to the imposed misfit strain of 0.14. The electric field has no dominant term and arises entirely as an induced polarization field and therefore is sensitive to the geometry because the abrupt changes in polarization at the material interfaces gives rise to the observed patterns.

Acknowledgement

This work was supported in part by the Air Force Office of Scientific Research (FA9550-06-1-0317).

References

[1] Q. Shen, S. Kycia, Phys. Rev. B 55 (1997) 15791.
[2] E. Tentarelli, J. Reed, Y.-P. Chen, W. Schaff, L. Eastman, J. Appl. Phys. 78 (1995) 4031.
[3] A. Ulyanenkov, N. Darowski, J. Grenzer, U. Pietsch, K. Wang, A. Forchel, Phys. Rev. B 60 (1999) 16701.
[4] A. Freundlich, A. Alemu, S. Bailey, Proc. 31st IEEE Photovoltaic Specialists Conference 2005, p. 137.
[5] R. Maranganti, P. Sharma, A review of strain field calculations in embedded quantum dots and wires, in: M. Reith, W. Schommers (Eds.), Handbook of Theoretical and Computational Nanotechnology, American Scientific, 2005 (Chapter 118).
[6] D. Faux, J. Downes, E. O'Reilly, J. Appl. Phys. 82 (1997) 3754.

[7] H. Johnson, L. Freund, Int. J. Solids Struct. 38 (2001) 1045.
[8] F. Glas, Philos. Mag. A. 82 (2002) 2591.
[9] X. Zhang, P. Sharma, Phys. Rev. B 72 (2005) 195345.
[10] H. Chu, J. Wang, J. Appl. Phys. 98 (2005) 034315.
[11] S. Mohammed, H. Morkoç, Prog. Quant. Electron. 20 (1996) 361.
[12] B. Jogai, J. Albrecht, E. Pan, J. Appl. Phys. 94 (2003) 3984.
[13] B. Jogai, J. Albrecht, E. Pan, J. Appl. Phys. 94 (2003) 6566.
[14] B. Jogai, J. Albrecht, E. Pan, Semicond. Sci. Tech. 19 (2004) 733.
[15] J. Davies, J. Appl. Phys. 84 (1998) 1358.
[16] S. Park, S. Chuang, Appl. Phys. Lett. 72 (1998) 3103.
[17] E. Pan, J. Appl. Phys. 91 (2002) 3785.
[18] E. Pan, J. Appl. Phys. 91 (2002) 6379.
[19] J. Davies, Appl. Phys. Lett. 75 (1999) 4142.
[20] E. Pan, J. Mech. Phys. Solids 52 (2004) 567.
[21] E. Pan, Proc. R. Soc. Lond. Ser. A 458 (2002) 181.
[22] E. Pan, F. Han, J. Albrecht, J. Appl. Phys. 98 (2005) 013534.